Indentation of a power law creeping solid

By A. F. Bower[1], N. A. Fleck[2], A. Needleman[1] and N. Ogbonna[2]

[1]*Division of Engineering, Brown University, Providence, Rhode Island 02912, U.S.A.*

[2]*Department of Engineering, University of Cambridge, Trumpington Street, Cambridge CB2 1PZ, U.K.*

The aim of this paper is to establish a rigorous theoretical basis for interpreting the results of hardness tests on creeping specimens. We investigate the deformation of a creeping half-space with uniaxial stress–strain behaviour $\dot{\epsilon} = \dot{\epsilon}_0(\sigma/\sigma_0)^m$, which is indented by a rigid punch. Both axisymmetric and plane indenters are considered. The shape of the punch is described by a general expression which includes most indenter profiles of practical importance. Two methods are used to solve the problem. The main results are found using a transformation method suggested by R. Hill. It is shown that the creep indentation problem may be reduced to a form which is independent of the geometry of the punch, and depends only on the material properties through m. The reduced problem consists of a nonlinear elastic half-space, which is indented to a unit depth by a rigid flat punch of unit radius (in the axisymmetric case), or unit semi-width (in the plane case). Exact solutions are given for $m = 1$ and $m = \infty$. For m between these two limits, the reduced problem has been solved using the finite element method. The results enable the load on the indenter and the contact radius to be calculated in terms of the indentation depth and rate of penetration. The stress, strain and displacement fields in the half-space may also be deduced. The accuracy of the solution is demonstrated by comparing the results with full-field finite element calculations. The predictions of the theory are shown to be consistent with experimental observations of hardness tests on creeping materials reported in the literature.

1. Introduction

An indentation test is a convenient method for measuring the mechanical properties of a material. Its most common application is to measure hardness. In the traditional hardness test, a diamond indenter is pressed into the surface of the solid with a prescribed load L, and either the depth of penetration h, or the radius of contact a is measured (see figure 1). Various shapes of indenter may be used in practice: the most common geometries are a sphere (Brinell test); a cone (Rockwell test) and a rectangular pyramid (Vickers test). The original form of the hardness test has been in use for over a century. However, there has been renewed interest in the method recently, as it may be used to measure the properties of very small samples of material. An instrument known as the nano-indenter has been developed, which applies a force of the order of 100 μN to the indenter, and can resolve penetration depths to within a fraction of a nanometer. This technique is used routinely to determine the properties of thin films of material used in the manufacture of microelectronic circuits (Nix 1989).

In principle, it is possible to determine the uniaxial stress versus strain behaviour

Proc. R. Soc. Lond. A (1993) **441**, 97–124
Printed in Great Britain

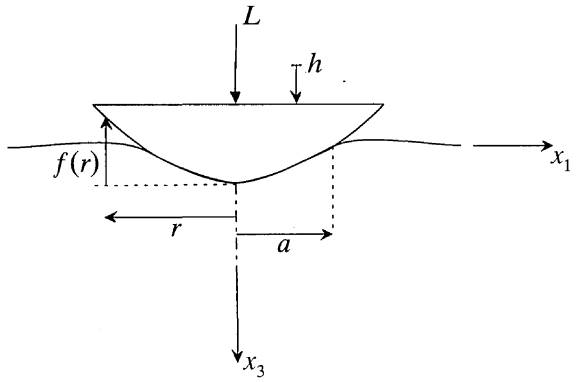

Figure 1. Punch indenting a half-space, showing notation and sign conventions.

of the specimen from the results of indentation tests. If the constitutive behaviour of the solid is independent of strain rate, its strain hardening characteristics may be deduced. It is also possible to determine the creep response of a rate dependent material, either by applying a fixed load to the indenter and measuring the rate of penetration, or by pressing the indenter into the specimen at a prescribed rate and measuring the load. Finally, the elastic modulus of the material may be found by measuring the compliance of the indenter during unloading.

For a rate independent material, the correlation between its strain hardening characteristics and indentation response is now well established. An empirical relation was found by Tabor (1951), who observed that if the uniaxial stress versus plastic strain curve for a material is fitted by a curve $\sigma = \sigma_0(\epsilon)^{1/m}$, the pressure under an indenter can be calculated as $L/(\pi a^2) \approx 3\sigma_0(\epsilon^{\text{eff}})^{1/m}$. The 'effective strain' ϵ^{eff} depends on the geometry of the indenter: Tabor proposed $\epsilon^{\text{eff}} = 0.2 \cot \beta$ for a cone or pyramid with included angle 2β. For a spherical indenter with diameter D, he suggested a value $\epsilon^{\text{eff}} = 0.4a/D$, where a is the radius of contact. A rigorous theoretical study of indentation of a power law hardening solid has been presented by Hill *et al.* (1989). They were able to predict *a priori* all of Tabor's empirical laws, and also studied in detail the nature of the deformation field beneath the indenter.

There have been several attempts to extend Tabor's empirical laws to rate dependent solids. For example, Mulhearn & Tabor (1960) suggested that for a power law creeping material with uniaxial response

$$\sigma = \sigma_0(\dot{\epsilon}/\dot{\epsilon}_0)^{1/m}, \tag{1.1}$$

the pressure under the indenter scales as

$$L/(\pi a^2) = \alpha\sigma_0(\gamma\dot{\epsilon}^{\text{eff}}/\dot{\epsilon}_0)^{1/m}. \tag{1.2}$$

Here, α and γ are material constants which vary with m, and the 'effective strain rate' $\dot{\epsilon}^{\text{eff}}$ depends on the geometry of the indenter, the contact radius a and the penetration rate $\dot{h}$. For a spherical indenter with diameter D, Mulhearn & Tabor proposed $\dot{\epsilon}^{\text{eff}} = \dot{a}/D$, where $\dot{a}$ is the rate of change of the radius of contact with time; Mayo & Nix (1988) used $\dot{\epsilon}^{\text{eff}} = \dot{h}/h$ for a pyramidal indenter. A measure of strain rate that applies to any indentor geometry has been proposed by Sargent & Ashby (1991), who suggested that $\dot{\epsilon}^{\text{eff}} = \dot{h}/\sqrt{A}$, where A is the area of contact.

Although a full analysis of creep under an indenter has not so far been attempted, some simple models have been developed. Atkins *et al.* (1965), and Wilkinson & Ashby (1975) used a technique developed by Marsh (1964) and Johnson (1970), in which the indenter is approximated by a cavity expanding in an infinite solid. They

predicted an expression of the form (1.1) for the indentation pressure, but they found $\dot{\epsilon}^{\text{eff}} = \dot{a}/a$. The calculations we present here suggest that the empirical formulae for $\dot{\epsilon}^{\text{eff}}$ proposed by Mulhearn & Tabor (1960), Mayo & Nix (1988) and Sargent & Ashby (1991) are more accurate. An alternative approach was used by Matthews (1980) to analyse the indentation of a creeping solid by a sphere. Guided by an exact solution for a linear viscous solid (Lee & Radok, 1960), and assuming that the pressure under the punch becomes uniform when $m = \infty$ in (1.2), he proposed an approximate expression for the contact pressure distribution for m between 1 and ∞. His analysis predicts that the indentation pressure varies according to (1.2), with $\dot{\epsilon}^{\text{eff}} = \dot{a}/D$. It is also possible to deduce the coefficients α and γ in (1.2) from his results. Although Matthews analysis is somewhat speculative, we will show here that his predictions are in reasonable agreement with more accurate numerical calculations.

In this paper, we present the results of a rigorous theoretical analysis of indentation creep. The problem to be solved is illustrated in figure 1: an infinite half-space, which occupies the region $x_3 \geqslant 0$, is loaded by a rigid punch. The material in the half-space is assumed to deform according to a nonlinear creep law of the form (1.1), which may be expressed in a more general way as

$$\frac{\dot{\epsilon}_{ij}}{\dot{\epsilon}_0} = \frac{3}{2}\left(\frac{\sigma_e}{\sigma_0}\right)^{m-1}\frac{S_{ij}}{\sigma_0}. \tag{1.3}$$

Here, $S_{ij} = \sigma_{ij} - \frac{1}{3}\delta_{ij}\sigma_{kk}$ is the deviatoric stress; $\sigma_e = (\frac{3}{2}S_{ij}S_{ij})^{\frac{1}{2}}$ denotes the von Mises effective stress and σ_0, $\dot{\epsilon}_0$ and m are material constants. In the limit $m = 1$ equation (1.3) represents a linear viscous (newtonian) solid, while if $m \to \infty$, equation (1.3) represents a rigid-perfectly plastic solid with yield stress σ_0. In practice, m usually lies between these two extremes, and (1.3) approximates the steady-state creep behaviour shown by many metals, polymers and ceramics.

Two general types of indenter will be considered. The punch may be axisymmetric, such as a cone or sphere, so that the area of contact is a circle of radius a. Alternatively, the indenter may be cylindrical, with its axis parallel to the surface of the half-space. Examples include a wedge, and a circular cylinder. In this case, the contact region is a line of width $2a$, and the half-space deforms in a state of plane strain. The profile of the punch $f(r)$ is assumed to have the form

$$f(r) = r^n/D^{n-1}, \tag{1.4}$$

where $n > 0$ and $D > 0$. The expression can be used to model several indenters of practical interest. For example, if we choose $n = 1$, and $D^{n-1} = \tan\beta$, then (1.4) describes a cone (for the axisymmetric case) or a wedge (for the plane problem), where 2β is the included angle at the apex. Alternatively, setting $n = 2$ in (1.4) approximates a sphere or circular cylinder of diameter $D \gg r$.

Friction may act between the indenter and the half-space. We will investigate two limiting cases here: that of a frictionless indenter; and that of a perfect adhesion, with no slip between the contacting surfaces.

For practical purposes, it is the variation of load L with indentation depth h and velocity $\dot{h}$ that is of greatest interest. This variation can only be found by calculating the stress and displacement fields under the punch. As part of the solution, it is necessary to find the variation of contact radius a with indentation depth. We will address these issues here, using two different methods of solution. Our main results will be obtained using an approach proposed by Hill (1992), who has shown that it

is possible to calculate the stress and velocity fields under a punch with profile given by (1.4) in a remarkably simple way, by noticing that the fields have certain self-similar properties. The analysis is reduced to calculating stresses and displacements in a nonlinear elastic solid, indented to a unit depth by a rigid flat punch of unit radius for the axisymmetric problem, or unit semi-width for the plane problem. Hill (1992) did not attempt to solve the reduced problem: our aim here is to provide the necessary numerical analysis. The accuracy of this approach will be demonstrated by comparing the predictions with full field finite element simulations.

The steps required to simplify the indentation problem are outlined in §2. The analysis leads to the following conclusions.

(*a*) *Variation of contact radius with indentation depth*

The contact radius a is related to the indentation depth by a constant c, where

$$h = \frac{1}{c^n}\frac{a^n}{D^{n-1}}. \tag{1.5}$$

The constant c is a function of the material constant m, the indenter parameter n, and depends weakly on the frictional conditions between the indenter and the half-space. It may be thought of as the ratio of the true to nominal contact radius, where the nominal contact radius is $(hD^{n-1})^{1/n}$ for a punch at depth h, from (1.4). This behaviour applies to both plane and axisymmetric indenters, although the value of c differs in the two cases.

(*b*) *Variation of load with penetration depth and velocity*

The load L applied to the punch is related to the indentation speed $\dot{h}$ by,

$$\frac{L}{\pi a^2 \sigma_0} = \left(\frac{\dot{h}}{a\dot{\epsilon}_0}\right)^{1/m} F_a(m) \quad \text{axisymmetric punch,} \tag{1.6}$$

$$\frac{L}{2a\sigma_0} = \left(\frac{\dot{h}}{a\dot{\epsilon}_0}\right)^{1/m} F_p(m) \quad \text{plane punch,} \tag{1.7}$$

where $F_a(m)$ and $F_p(m)$ are functions which depend only upon the material parameter, m, and are independent of the shape of the indenter. They depend weakly on the magnitude of the coefficient of friction between the punch and the half-space.

(*c*) *Displacement, strain and stress fields*

The stress and strain rate fields in the solid have the form

$$\sigma_{ij}(x_k) = \sigma_0(\dot{h}/a\dot{\epsilon}_0)^{1/m}\,\Sigma_{ij}(m, x_k/a), \tag{1.8}$$

$$\dot{\epsilon}_{ij} = (\dot{h}/a)\,E_{ij}(m, x_k/a), \tag{1.9}$$

where Σ_{ij} and E_{ij} are functions which are independent of the geometry of the punch, and only depend on the material properties through m. They are also weak functions of friction. The form of equations (1.8) and (1.9) follows from the observation that the strain rates and stresses in a pure creeping solid are independent of the history of loading, and depend only on the instantaneous velocities prescribed on the surface. Therefore, σ_{ij} and $\dot{\epsilon}_{ij}$ are identical to the stress and strain rate fields under a rigid flat punch of width a, which indents a half-space at a velocity $\dot{h}$. The scaling of $\dot{\epsilon}_{ij}$ and σ_{ij} with $\dot{h}$ and a can be deduced by dimensional analysis.

The form of the displacement and strain fields under a curved punch is less obvious. We will show that

$$u_i(x_k) = (a/D)^{n-1}\, a\tilde{u}_i(m, n, x_k/a), \tag{1.10}$$

$$\epsilon_{ij}(x_k) = (a/D)^{n-1}\, \tilde{\epsilon}_{ij}(m, n, x_k/a), \tag{1.11}$$

where $\tilde{u}_i$ and $\tilde{\epsilon}_{ij}$ are functions which depend on the geometry of the punch through n and material properties through m, but are independent of indentation depth.

Furthermore, we will show that c, $F_a(m)$, $F_p(m)$, Σ_{ij} and E_{ij} may be determined by solving the following reduced contact problem. A nonlinear elastic half-space, with constitutive law:

$$\epsilon_{ij} = \tfrac{3}{2}\sigma_e^{m-1} S_{ij} \tag{1.12}$$

is subjected to a unit displacement normal to its surface over the region $|\hat{r}| = (\hat{x}_1^2 + \hat{x}_2^2)^{\frac{1}{2}} \leqslant 1$ for the axisymmetric case, or $|\hat{x}_1| \leqslant 1$ in the case of a plane indenter. The frictional conditions in the reduced problem are the same as those in the original creep problem: either full slip or perfect adhesion. Suppose that the resulting displacement of the surface is $U_3(\hat{r})$, and the contact pressure on $|\hat{r}| \leqslant 1$ is $P(\hat{r})$. Then $c(m, n)$ for indentation of the creeping half-space follows as,

$$c^n = 1 - n\int_1^\infty \frac{U_3(\hat{r})}{\hat{r}^{n+1}}\,\mathrm{d}\hat{r}. \tag{1.13}$$

In addition, F_p and F_a are given by

$$F_a(m) = 2\int_0^1 P(\hat{r})\,\hat{r}\,\mathrm{d}\hat{r} \quad \text{axisymmetric punch,} \tag{1.14}$$

$$F_p(m) = \int_0^1 P(\hat{r})\,\mathrm{d}\hat{r} \qquad \text{plane punch.} \tag{1.15}$$

Finally, Σ_{ij} and E_{ij} are the stress and strain fields in the nonlinear elastic half-space.

For the special case of a linear viscous solid ($m = 1$), this method has been used to derive exact solutions for both axisymmetric and plane indenters of arbitrary profile. For a rigid plastic solid ($m = \infty$), exact solutions have been calculated for plane indenters. For m between these cases, we have solved the reduced problem using the finite element method. The results have been used to calculate c, F_a, F_p, Σ_{ij} and E_{ij} for spherical and conical (axisymmetric) indenters, and also circular cylindrical and wedge (plane) indenters. The calculations show that the indentation load is closely approximated by Tabor's empirical law given in (1.2). We will also show that the predictions of our analysis are in good agreement with experimental results reported in the literature.

2. Theory

We begin our analysis by stating the equations and boundary conditions governing the displacement, strain and stress fields in the creeping half-space loaded by a rigid punch, as illustrated in figure 1. Provided that the indentation depth is small and the indenter is blunt, so that $D^{n-1} \gg a$, we may assume that the displacements and strains under the indenter are infinitesimal. In this case, the strains ϵ_{ij} are related to the displacements u_i by

$$\epsilon_{ij} = \tfrac{1}{2}(u_{i,j} + u_{j,i}), \tag{2.1}$$

where the comma denotes differentiation in the usual manner. The stress field σ_{ij} is related to the strain by the constitutive law given in equation (1.3). The stresses must satisfy equilibrium: $\sigma_{ij,j} = 0$.

For a punch of profile (1.4), indenting a creeping half-space of constitutive description (1.3), the boundary conditions are

$$u_3 = h - (r^n/D^{n-1}), \quad \dot{u}_3 = \dot{h}, \quad |r| \leqslant a, \tag{2.2}$$

$$\sigma_{33} = \sigma_{13} = \sigma_{23} = 0, \quad |r| \geqslant a. \tag{2.3}$$

The frictional conditions between the punch and the half-space are specified by the following boundary conditions:

$$\sigma_{13} = \sigma_{23} = 0, \quad |r| \leqslant a, \quad \text{frictionless punch}, \tag{2.4}$$

$$\dot{u}_1 = \dot{u}_2 = 0, \quad |r| \leqslant a, \quad \text{sticking punch}. \tag{2.5}$$

In writing the boundary conditions (2.2)–(2.5), we have used the convention that r denotes $r = (x_1^2 + x_2^2)^{\frac{1}{2}}$ for the axisymmetric punch, while $r = x_1$ for the plane punch. In the case of a plane indenter, we also assume a state of plane strain in the half-space, such that $u_2 = \epsilon_{22} = 0$, with u_1 and u_3 independent of x_2. Finally we assume that the stresses vanish at infinity, and that the deformed profile of the half-space is smooth at $r = a$. The latter condition guarantees that there is no overlap between the indenter and the half-space for $r \geqslant a$.

Two approaches may be used to solve the creep indentation problem. We may solve it directly using the finite element method, or alternatively we may first simplify the problem by transforming the governing equations and boundary conditions, as discussed by Hill *et al.* (1989) and Hill (1992). We will initially adopt the latter approach.

(*a*) *Similarity transformation*

We begin by observing that at any particular instant the velocity, strain rate and stress fields in the half-space only depend on the size of the contact a and the indentation rate $\dot{h}$, and are independent of the history of loading. The fields are identical to the velocities and stresses which would be induced in the creeping half-space by a *flat* punch of size a, indenting the surface at a rate $\dot{h}$. They depend on the shape of the indenter only to the extent that the contact size a is determined by the geometry of the punch. It is natural, therefore, to express the fields in terms of dimensionless distances $\hat{x}_i = x_i/a$. In particular, we consider scaling the displacement boundary condition (2.2) to the form

$$\frac{u_3 D^{n-1}}{a^n} = \frac{hD^{n-1}}{a^n} - \hat{r}^n, \quad \hat{r} \leqslant 1, \tag{2.6}$$

where $\hat{r} = (\hat{x}_1^2 + \hat{x}_2^2)^{\frac{1}{2}}$ for the axisymmetric case, and $\hat{r} = |\hat{x}_1|$ for a plane indenter. This may be simplified by defining

$$\tilde{u}_i = u_i D^{n-1}/a^n, \quad c = (a^n/hD^{n-1})^{1/n}, \tag{2.7}$$

so that (2.6) becomes

$$\tilde{u}_3 = (1/c^n) - \hat{r}^n, \quad \hat{r} \leqslant 1. \tag{2.8}$$

At this point, we assume without proof that $\tilde{u}_i(\hat{x}_k)$ and c as defined in (2.7) are independent of indentation depth. These assumptions will be verified shortly. Treating $\tilde{u}_i(\hat{x}_k)$ as a displacement field, we define an associated strain field as

$$\tilde{\epsilon}_{ij} = \frac{1}{2}\left(\frac{\partial \tilde{u}_i}{\partial \hat{x}_j} + \frac{\partial \tilde{u}_j}{\partial \hat{x}_i}\right). \tag{2.9}$$

Since $\tilde{u}_i(\hat{x}_k)$ have been assumed to be independent of indentation depth, it follows that $\tilde{\epsilon}_{ij}(\hat{x}_k)$ are similarly invariant. Noting that $(\partial/\partial\tilde{x}_k) \equiv (a\,\partial/\partial x_k)$ it follows from the definition of $\tilde{u}_i$ in (2.7) that

$$\tilde{\epsilon}_{ij} = (D/a)^{n-1}\,\epsilon_{ij}. \tag{2.10}$$

The stress field $\sigma_{ij}(\hat{x}_k)$ may now be found in terms of the transformed strains $\tilde{\epsilon}_{ij}(\hat{x}_k)$, through the constitutive law given in (1.3). To this end, we first calculate the strain rate $\dot{\epsilon}_{ij}(x_k)$ at a material point x_k, in terms of $\tilde{\epsilon}_{ij}$. Differentiating (2.10) with respect to time gives

$$\dot{\epsilon}_{ij} = (n-1)\frac{a^{n-2}}{D^{n-1}}\dot{a}\tilde{\epsilon}_{ij} + \left(\frac{a}{D}\right)^{n-1}\frac{\partial\tilde{\epsilon}_{ij}}{\partial\hat{x}_k}\frac{\partial\hat{x}_k}{\partial t}, \tag{2.11}$$

where we have made use of the assumption that $\tilde{\epsilon}_{ij}(\hat{x}_k)$ is independent of time for fixed $\hat{x}_k$. Noting that

$$\frac{\partial\hat{x}_k}{\partial t} = \frac{\partial(x_k/a)}{\partial a}\dot{a} = -\frac{\dot{a}}{a}\hat{x}_k, \tag{2.12}$$

we may simplify (2.11) to

$$\dot{\epsilon}_{ij} = \left(\frac{a}{D}\right)^{n-1}\frac{\dot{a}}{a}\left((n-1)\,\tilde{\epsilon}_{ij} - \hat{x}_k\frac{\partial\tilde{\epsilon}_{ij}}{\partial\hat{x}_k}\right). \tag{2.13}$$

In the same way, the velocity of a particle $\dot{u}_i(x_k)$ at a material point x_k may be expressed in terms of the steady field $\tilde{u}_i(\hat{x}_k)$, by differentiating the first equation in (2.6). This leads to

$$\dot{u}_i = \left(\frac{a}{D}\right)^{n-1}\dot{a}\left(n\tilde{u}_i - \hat{x}_k\frac{\partial\tilde{u}_i}{\partial\hat{x}_k}\right). \tag{2.14}$$

In principle, the transformed strain field $\tilde{\epsilon}_{ij}$ may now be calculated by substituting $\dot{\epsilon}_{ij}$ from (2.13) into the constitutive law (1.3) and using the equilibrium equation, together with appropriate boundary conditions. However, it is possible to simplify the governing equations still further, by defining new measures of displacement and strain as

$$\hat{u}_i = n\tilde{u}_i - \hat{x}_k\frac{\partial\tilde{u}_i}{\partial\hat{x}_k}, \tag{2.15}$$

$$\hat{\epsilon}_{ij} = (n-1)\,\tilde{\epsilon}_{ij} - \hat{x}_k\frac{\partial\tilde{\epsilon}_{ij}}{\partial\hat{x}_k}. \tag{2.16}$$

Using these definitions, we may rewrite equations (2.13) and (2.14) as

$$\dot{\epsilon}_{ij} = (a/D)^{n-1}\,(\dot{a}/a)\,\hat{\epsilon}_{ij}, \tag{2.17}$$

$$\dot{u}_i = (a/D)^{n-1}\,\dot{a}\hat{u}_i. \tag{2.18}$$

The stress field may now be written in terms of $\hat{u}_i$ and $\hat{\epsilon}_{ij}$. Inverting the constitutive law (1.3) gives

$$\frac{S_{ij}}{\sigma_0} = \frac{2}{3}\left(\frac{\dot{\epsilon}_e}{\dot{\epsilon}_0}\right)^{(1-m)/m}\frac{\dot{\epsilon}_{ij}}{\dot{\epsilon}_0}. \tag{2.19}$$

Next, introduce a new stress quantity $\hat{\sigma}_{ij}(\tilde{x}_k)$, defined by

$$\hat{\sigma}_{ij}(x_k/a) = \left[\left(\frac{a}{D}\right)^{n-1}\frac{\dot{a}}{a\dot{\epsilon}_0}\right]^{-1/m}\frac{\sigma_{ij}(\hat{x}_k)}{\sigma_0}, \tag{2.20}$$

where $\dot{\epsilon}_e = (\frac{2}{3}\dot{\epsilon}_{ij}\,\dot{\epsilon}_{ij})^{\frac{1}{2}}$ is the von Mises effective strain rate. The constitutive relation becomes,

$$\hat{S}_{ij} = \tfrac{2}{3}\hat{\epsilon}_e^{(1-m)/m}\,\hat{\epsilon}_{ij}, \tag{2.21}$$

where $\hat{\epsilon}_e = (\frac{2}{3}\hat{\epsilon}_{ij}\,\hat{\epsilon}_{ij})^{\frac{1}{2}}$. This is the stress–strain law for a power law elastic body.

Finally, we may write the complete set of equations and boundary conditions which determine the fields in the creeping half-space in terms of the invariant fields $\hat{u}_i$. The strain-displacement relations (2.1) become

$$\hat{\epsilon}_{ij} = \frac{1}{2}\left(\frac{\partial \hat{u}_i}{\partial \hat{x}_j} + \frac{\partial \hat{u}_j}{\partial \hat{x}_i}\right) \tag{2.22}$$

and the equilibrium equations $\sigma_{ij,j} = 0$ become

$$\partial \hat{\sigma}_{ij}/\partial \hat{x}_j = 0. \tag{2.23}$$

The boundary conditions (2.3)–(2.5) may be rewritten as

$$\hat{u}_3 = n/c^n, \quad \hat{u}_3 = (\dot{h}/\dot{a})\,(D/a)^{n-1}, \quad |\hat{r}| < 1, \tag{2.24}$$

$$\hat{\sigma}_{33} = \hat{\sigma}_{23} = \hat{\sigma}_{13} = 0, \qquad |\hat{r}| > 1 \tag{2.25}$$

and

$$\hat{\sigma}_{13} = \hat{\sigma}_{23} = 0, \quad |r| \leqslant 1, \quad \text{frictionless punch}, \tag{2.26}$$

$$\hat{u}_1 = \hat{u}_2 = 0, \quad |r| \leqslant 1, \quad \text{sticking punch}, \tag{2.27}$$

where $\hat{r} = (\hat{x}_1^2 + \hat{x}_2^2)^{\frac{1}{2}}$ for the axisymmetric punch, and $\hat{r} = |\hat{x}_1|$ for the plane punch, as before. The first of the boundary conditions on $\hat{u}_3$ in (2.24) has been obtained using the relationship between the displacement fields $\hat{u}_i$ and $\tilde{u}_i$ given in (2.15), together with the boundary condition on $\tilde{u}_3$ in (2.8). The second is a consequence of the boundary condition on $\dot{u}_3$ in (2.2), which has been rewritten by expressing $\dot{u}_3$ in terms of $\hat{u}_3$ using (2.18). Their equivalence verifies our initial assumption that c as defined in (2.7) is a constant. For on equating the two expressions for $\hat{u}_3$ in (2.24) and substituting for c^n using (1.5) we find that

$$\dot{h}/h = n\dot{a}/a. \tag{2.28}$$

Integrating (2.28) and comparing the result with (1.5) shows that c is indeed constant. In addition, we note that (2.14) may be used to verify our assumption that $\tilde{u}_i$ is independent of indentation depth. Since c is independent of h, it follows from (1.5) that $\dot{a}(a/D)^{n-1}$ is proportional to $\dot{h}$. The velocity field $\dot{u}_i$ is known to be independent of h, and is also proportional to $\dot{h}$, showing that $\tilde{u}_i$ cannot depend on indentation depth.

Equations (2.22)–(2.27), together with the stress–strain relation in (2.21) may be taken to be conditions defining the transformed displacement field $\hat{u}_i$. They are identical to the equations that determine the fields in a power-law elastic half-space, which has a rigid flat punch of unit width pressed into its surface to a depth n/c^n. The frictional conditions on the flat punch are identical to those on the curved indenter in the original creep problem.

A suitable method for solving the nonlinear elastic punch problem will be given shortly. For the moment, suppose that $U_i(\hat{x}_k)$, $E_{ij}(\hat{x}_k)$ and $\Sigma_{ij}(\hat{x}_k)$ denote the displacements, strains and stresses in a half-space with constitutive law (2.21), which has a flat punch of unit radius (in the axisymmetric case) or unit semi-width (in the plane problem), pressed into its surface to a unit depth. The transformed fields $\hat{u}_i$, $\hat{\epsilon}_{ij}$ and $\hat{\sigma}_{ij}$ follow as

$$\hat{u}_i(\hat{x}_k) = (n/c^n)\,U_i(\hat{x}_k), \tag{2.29}$$

$$\hat{\epsilon}_{ij}(\hat{x}_k) = (n/c^n)\,E_{ij}(\hat{x}_k), \tag{2.30}$$

$$\hat{\sigma}_{ij}(\hat{x}_k) = (n/c^n)^{1/m}\,\Sigma_{ij}(\hat{x}_k). \tag{2.31}$$

On substituting into equations (2.17) and (2.20) and using the definition of c in (2.7), we obtain the expressions for stresses and strain rates given in (1.8) and (1.9) of the Introduction. The indentation load L is then found by integrating the stresses over the area of contact. Using $p(r)$ to denote the contact pressure on the creeping half-space, we have

$$L = 2\pi \int_0^a p(r)\, r\, \mathrm{d}r, \quad \text{axisymmetric punch,} \tag{2.32}$$

$$L = 2 \int_0^a p(r)\, r\, \mathrm{d}r, \quad \text{plane punch.} \tag{2.33}$$

This may be written in terms of the corresponding contact pressure for the nonlinear elastic indentation problem, which we denote by $P(\hat{r})$. The pressures are related by

$$p(r) = \sigma_0 (\dot{h}/a\dot{\epsilon}_0)^{1/m} P(\hat{r}), \tag{2.34}$$

whereupon (2.32) and (2.33) may be written in the form given in (1.6) and (1.7), with F_a and F_p as defined in (1.14) and (1.15). We note that F_a and F_p correspond to the loads applied to the flat punch in the nonlinear elasticity problem.

To complete our analysis, we show that c may be determined from the solution to the nonlinear elastic punch problem using the expression given in (1.13). With this in mind, we first calculate the steady displacement field $\tilde{u}_i$ in terms of the displacements U_i in the nonlinear elastic half-space. They are related by equations (2.15) and (2.29), which may be integrated by first writing

$$n\tilde{u}_i - \hat{x}_k \frac{\partial \tilde{u}_i}{\partial \hat{x}_k} \equiv -(\hat{x}_j \hat{x}_j)^{n/2} \hat{x}_k \frac{\partial}{\partial \hat{x}_k} ((\hat{x}_p \hat{x}_p)^{-n/2} \hat{u}_i(\hat{x}_m)) = \frac{n}{c^n} U_i(\hat{x}_m), \tag{2.35}$$

so that

$$\tilde{u}_i(\hat{x}_m) = \frac{n(\hat{x}_k \hat{x}_k)^{n/2}}{c^n} \int_C \frac{U_i(\xi_j(s))}{s^{n+1}} \mathrm{d}s. \tag{2.36}$$

Here, the path of integration $\xi_j(s)$ is a radial line from the point $\hat{x}_k$ to infinity. In particular, the displacement at a point $\hat{r} = \hat{R}$ on the surface is found to be

$$\tilde{u}_i(\hat{R}) = \frac{n\hat{R}^n}{c^n} \int_{\hat{R}}^{\infty} \frac{U_i(\hat{r})}{\hat{r}^{n+1}} \mathrm{d}\hat{r}. \tag{2.37}$$

Evaluating $\tilde{u}_3$ at $\hat{r} = 1$ and substituting into the boundary condition (2.8) then gives

$$\frac{n}{c^n} \int_1^{\infty} \frac{U_i(\hat{r})}{\hat{r}^{n+1}} \mathrm{d}\hat{r} = \frac{1}{c^n} - 1 \tag{2.38}$$

which may be re-arranged to give the expression given for c^n in equation (1.13).

A physical interpretation for c was given in the introduction: it determines the ratio of the true to nominal contact area under the punch. We now see that it has a second interpretation, in that it controls the vertical displacement of the surface at the edge of the contact area. Evaluating (2.8) at $\hat{r} = 1$ and using (2.7), we find that

$$u_3(a) = h(1 - c^n). \tag{2.39}$$

The displacement $u_3(a)$ evidently varies linearly with indentation depth h, and c^n determines its magnitude. If $c < 1$, material is pushed into the surface at the edge of the contact, while if $c > 1$, material piles up at the side of the indentation.

It is interesting to note that the tangential displacement at the edge of the contact area varies in a similar way. Equations (2.37) and (2.7) show that $u_1(a) = hb(m, n)$, where $b(m, n)$ is given by

$$b(m, n) = \int_1^\infty \frac{U_1(\hat{r})}{\hat{r}^{n+1}} \mathrm{d}\hat{r}. \tag{2.40}$$

The tangential displacement at the edge of the contact therefore also varies linearly with h. The constant b plays a similar role to c in that it determines the magnitude of the displacement. Like c, it depends only on the indenter shape through n and material properties through m, and is a weak function of friction. For a perfectly bonded indenter, b also controls the variation of tangential displacement inside the area of contact. Noting that in this case $\dot{u}_1(r) = 0$ for $r \leqslant a$, it follows that

$$u_1(r) = \frac{b}{c^n} \frac{r^n}{D^{n-1}}, \quad r \leqslant a. \tag{2.41}$$

(b) *Solutions for linear viscous and rigid perfectly plastic solids*

For some values of m exact solutions to the creep indentation problem may be found using the method outlined in the preceding section. It is convenient to solve the problem for axisymmetric and plane indenters separately.

(i) *Axisymmetric punch, $m = 1$*

For axisymmetric indenters, an exact solution may be found for a rigid punch of profile given by (1.4) indenting a linear viscous solid. For such a material, we set $m = 1$ in the constitutive law (1.3), whereupon the constitutive model for the transformed problem (1.12) becomes

$$\epsilon_{ij} = \tfrac{3}{2} S_{ij}. \tag{2.42}$$

This is the expression for an incompressible linear elastic solid with unit Young's modulus. The fields U_i, E_{ij} and Σ_{ij} are therefore given by the displacements, strains and stresses in an incompressible linear elastic half-space which has a flat axisymmetric punch of unit radius pushed a unit distance into its surface. The solution to this problem is given in Sneddon (1951), and has been expressed in terms of elementary functions by Fabrikant (1990). Conveniently, the results are independent of the friction between the punch and the half-space. However, the full equations for the displacement and stress fields are lengthy, and will not be repeated here. We merely note that the displacement and contact pressure at the surface $x_3 = 0$ are given by

$$U_3(\hat{r}) = (2/\pi) \arcsin(1/\hat{r}), \quad \hat{r} > 1, \tag{2.43}$$

$$U_1(\hat{r}) = U_2(\hat{r}) = 0, \quad \hat{r} < 1, \tag{2.44}$$

$$P(\hat{r}) = (4/3\pi)(1 - \hat{r}^2)^{-\frac{1}{2}}, \quad \hat{r} < 1. \tag{2.45}$$

The dimensionless contact pressure $F_a(m)$ for $m = 1$ may then be calculated using equation (1.14), which gives $F_a(1) = 8/3\pi$. The ratio of true to nominal contact areas c can be found by substituting for U_3 in (1.13). Although the integral can be evaluated exactly for any integer value of n, the results are somewhat cumbersome and we only give results for two cases of practical interest. They are

$$c = \begin{cases} 2/\pi, & \text{conical indenter } (n = 1), \\ 1/\sqrt{2}, & \text{spherical indenter } (n = 2). \end{cases} \tag{2.46}$$

Using the values of c, we may write out in full the variation of contact radius and load with depth for conical and spherical indenters. For the cone with apex angle 2β, we set $D^{n-1} = \tan\beta$ and $n = 1$ in (1.5), while for the sphere of diameter D we set $n = 2$. This gives

$$a = \begin{cases} 2h\tan\beta/\pi, & \text{conical indenter,} \\ (Dh/2)^{\frac{1}{2}}, & \text{spherical indenter} \end{cases} \tag{2.47}$$

and

$$\frac{L}{\pi a^2\sigma_0} = F(m=1)\left(\frac{\dot{h}}{a\dot{\epsilon}_0}\right) = \frac{8}{3\pi}\left(\frac{\dot{h}}{a\dot{\epsilon}_0}\right), \tag{2.48}$$

$$= \frac{4}{3}\frac{\dot{h}}{h\dot{\epsilon}_0}\frac{1}{\tan\beta} \quad \text{conical indenter,} \tag{2.49}$$

$$= \frac{16}{3\pi}\frac{a}{D}\frac{\dot{h}}{h\dot{\epsilon}_0} \quad \text{spherical indenter.} \tag{2.50}$$

The same results were found by Lee & Radok (1960) using a different method.

(ii) *Plane punch, $m = 1$*

A similar procedure may be used to calculate the fields under a plane indenter. In this case, the reduced contact problem consists of an incompressible half-space with unit Young's modulus, which has a plane flat punch of unit semi-width pressed a unit distance into its surface. The solution to this problem illustrates a difficulty with applying the transformation procedure to plane indentation of linear creeping solids. Formally, the elastic solution is $U_3(\hat{r}) = 1$ for all values of $\hat{r}$, and we also find $P(\hat{r}) = 0$. Consequently, both $c = 0$ and $F_p(m) = 0$ for $m = 1$. This result is not surprising: it is well known that if a finite load is applied to a plane punch indenting a linear elastic solid, the displacement under the indenter is infinite, and we would expect the same result for a linear creeping solid. We therefore accept that $c = 0$ in this case, and rewrite the expression for the load (1.7) in terms of $\dot{a}$ rather than $\dot{h}$

$$\frac{L}{2a\sigma_0} = \left(\frac{\dot{a}}{a}\frac{na^{n-1}}{\dot{\epsilon}_0 D^{n-1}}\right)^{1/m}\frac{F_p(m)}{c^{n/m}}. \tag{2.51}$$

The ratio $F_p(m)/c^{n/m}$ can be shown to tend to a well-defined limit as $m \to 1$. However, this limit cannot be calculated easily using the scaling procedure, and it is simpler to calculate the indentation pressure using the methods given in Lee & Radok (1960). In particular, it may be shown that for a wedge shaped indenter with included angle 2β ($D^{n-1} = \tan\beta, n = 1$), and a cylindrical indenter diameter D ($n = 2$),

$$\frac{L}{2a\sigma_0} = \frac{\pi}{3}\left(\frac{\dot{a}}{a\dot{\epsilon}_0\tan\beta}\right), \quad \text{wedge indenter,} \tag{2.52}$$

$$\frac{L}{2a\sigma_0} = \frac{4\pi}{3}\left(\frac{\dot{a}}{\dot{\epsilon}_0 D}\right), \quad \text{circular cylindrical indenter.} \tag{2.53}$$

(iii) *Plane punch, $m = \infty$*

For a plane indenter, an exact solution can also be found for $m = \infty$, which represents a rigid perfectly plastic solid. Consequently, the transformed fields are found from the solution to a rigid perfectly plastic solid with unit tensile yield stress, indented to unit depth by a rigid flat punch. Slip-line field solutions to this problem

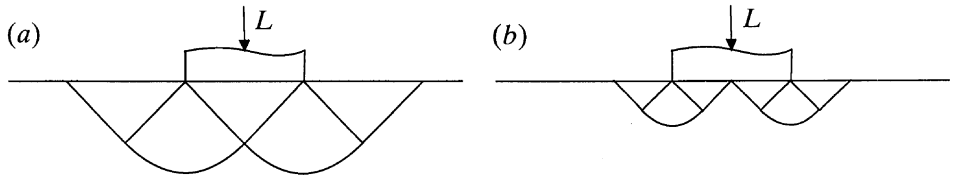

Figure 2. Slip line field solutions for a plane flat punch indenting a rigid plastic solid. (*a*) Hill's solution. (*b*) Prandtl's solution.

have been found by Prandtl (1920) and Hill (1949), and are illustrated in figure 2. In Hill's solution, the material in the contact area does not move tangentially relative to the face of the punch, so we have assumed that this is the solution to the perfectly bonded case. In Prandtl's solution, material under the punch is displaced laterally, so we have used his solution for the frictionless indenter. However, since the surface is free of tangential traction in both cases, Hill's field is also an admissible solution to the frictionless indentation problem, so our distinction is arbitrary. The contact pressure distribution for both solutions is

$$P(\hat{r}) = (2+\pi)/\sqrt{3}, \quad |\hat{r}| < 1, \tag{2.54}$$

while the displacements at the surface are

$$U_3 = \begin{cases} 1, 0 < |\hat{r}| < 1;\ -\frac{1}{2}, 1 < |\hat{r}| < 3;\ 0, 3 < |\hat{r}|; & \text{bonded punch,} \\ 1, 0 < |\hat{r}| < 1;\ -1, 1 < |\hat{r}| < 2;\ 0, 1 < |\hat{r}|; & \text{frictionless punch,} \end{cases} \tag{2.55}$$

$$U_1 = \begin{cases} 0, 0 < |\hat{r}| < 1;\ \frac{1}{2}, 1 < |\hat{r}| < 3;\ 0, 2 < |\hat{r}|; & \text{bonded punch,} \\ 1, 0 < |\hat{r}| < 2;\ 0, 2 < |\hat{r}|; & \text{frictionless punch.} \end{cases} \tag{2.56}$$

We find that $F_p(m \to \infty) = (2+\pi)/\sqrt{3}$, while c and b are given by

$$c^n = \begin{cases} \frac{1}{2}(3-3^{-n}), & \text{bonded punch,} \\ 2-2^{-n}, & \text{frictionless punch,} \end{cases} \tag{2.57}$$

$$b = \begin{cases} \frac{1}{2}(1-3^{-n}), & \text{bonded punch,} \\ 1-2^{-n}, & \text{frictionless punch.} \end{cases} \tag{2.58}$$

(*c*) *Numerical analysis*

For m between the two limiting cases discussed in the preceding section, the solution to the reduced contact problem has been calculated using the finite element method. The numerical procedure which we have used is described in detail in Shih & Needleman (1984), and will only be briefly summarized here. The conventional displacement based finite element method cannot be used to analyse deformation in incompressible materials. To avoid this difficulty, a reduced integration penalty method has been used: the nonlinear elastic constitutive law (2.21) has been approximated by a compressible elastic–plastic solid, and the incompressible limit has been approached numerically. Thus, the strain has been written as the sum of a compressible elastic part $\epsilon^{\mathrm{e}}_{ij}$ and a volume preserving plastic part $\epsilon^{\mathrm{p}}_{ij}$, which are related to the stresses by

$$\epsilon^{\mathrm{e}}_{ij} = \frac{1+\nu}{E} S_{ij} + \frac{1-2\nu}{3E} \sigma_{kk}\, \delta_{ij}, \tag{2.59}$$

$$\epsilon^{\mathrm{p}}_{ij} = \frac{3}{2}\left(\frac{1}{E_{\mathrm{s}}} - \frac{1}{E}\right) S_{ij}, \tag{2.60}$$

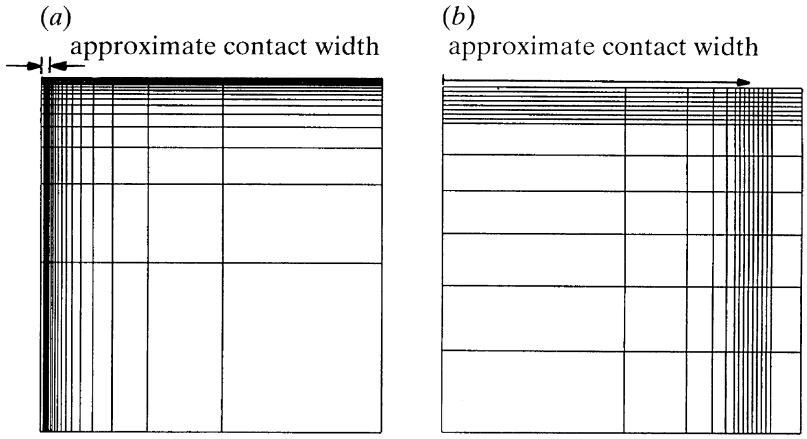

Figure 3. Typical finite element mesh used to solve flat punch problem. (*a*) Full mesh. (*b*) Mesh close to area of contact.

where ν is Poissons ratio, E_s is the ratio of stress to strain in uniaxial tension, and E is the slope of the stress–strain curve at $\epsilon = 0$. The incompressible limit has been approximated using a value of $\nu = 0.49999$. In addition, the uniaxial stress–strain curve has been represented by a piecewise power hardening law:

$$\frac{\epsilon}{\epsilon_0} = \frac{m}{m-1} - \left[\frac{1+m^2}{(m-1)^2} - \left(\frac{\sigma}{\sigma_0} + \frac{1}{m-1}\right)^2\right]^{\frac{1}{2}}, \quad \epsilon < \epsilon_0, \tag{2.61}$$

$$\frac{\epsilon}{\epsilon_0} = \left(\frac{\sigma}{\sigma_0}\right)^m, \quad \epsilon \geqslant \epsilon_0. \tag{2.62}$$

This form of the stress–strain curve gives the required power-law hardening behaviour for $\epsilon \geqslant \epsilon_0$, but has a finite slope at $\epsilon = 0$, which improves the convergence of the numerical procedure. To obtain pure power-law hardening behaviour, it is necessary to ensure that all strains exceed ϵ_0. In an indentation problem, there is always a region distant from the punch where this is not the case, but numerical tests have shown that the results are not sensitive to the value chosen for ϵ_0. In our calculations, we have used values $\epsilon_0 = \sigma_0 = 0.001$, and scaled the results appropriately to match the constitutive behaviour required by equation (2.21).

A modified Newton–Raphson method has been used to solve the nonlinear boundary value problem outlined in §2*b*. The method is based on an expansion of the principle of virtual work about an approximation to the required solution, which gives

$$\int_V [\Delta S_{ij}\,\delta e_{ij} + \tfrac{1}{3}\Delta\sigma_{kk}\,\delta\epsilon_{ll}]\,\mathrm{d}V - \int_A \Delta\sigma_{ij}\,n_j\,\delta u_i\,\mathrm{d}A$$

$$= -\int_V [S_{ij}\,\delta e_{ij} + \tfrac{1}{3}\sigma_{kk}\,\delta\epsilon_{ll}]\,\mathrm{d}V + \int_A \sigma_{ij}\,n_j\,\delta u_i\,\mathrm{d}A, \tag{2.63}$$

where $e_{ij} = \epsilon_{ij} - \frac{1}{3}\epsilon_{kk}$ are the deviatoric strains, S_{ij} and σ_{ij} are the current approximation to the stress field, and ΔS_{ij} and Δe_{ij} are a correction to the current state of stress and strain. Equation (2.63) is solved repeatedly for the displacement variations until a convergent solution is reached.

The Newton–Raphson scheme converges quadratically if the initial estimate of the

solution is sufficiently close to the actual solution. We have used parameter tracking to generate accurate initial estimates. In this approach, a solution is obtained for $m = 1$, which is then used as an initial estimate for a higher value of m. In this way, solutions are found for progressively increasing values of m. This method works well for values of $m < 5$, but we were unable to obtain a converged solution for $m > 5$. For higher values of m, we have used a relaxation method to calculate a solution. Equation (2.63) is solved for a correction to the displacement field Δu_i. At each iteration the displacements are updated as $u_i^{(n+1)} = u_i^{(n)} + \alpha \Delta u_i$, where α is an adjustable parameter. Using a value between 0.25 and 0.5 for α, we have been able to find solutions for values of m up to 1000.

The displacements in (2.63) have been approximated using axisymmetric and plane quadratic elements. The full lagrangian shape functions are necessary for approaching the incompressible limit (Malkus & Hughes, 1978). The deviatoric and volumetric terms in the volume integrals in (2.63) were evaluated separately: 3×3 gaussian integration was used for the deviatoric terms, while the volumetric terms were evaluated using 2×2 Gauss points.

Where we report results for stresses in the solid, the deviatoric stress components were calculated at the 3×3 integration points, while the hydrostatic component was evaluated at the 2×2 Gauss points, and extrapolated to the 3×3 points using the bilinear shape functions. This approach gave good results for the frictionless indenter, but for the fully bonded case we found some oscillations in the hydrostatic stress, particularly near the edge of the area of contact. In this case, the stress field was estimated by combining the average value of the hydrostatic pressure at the 2×2 Gauss points with the deviatoric stresses at the 3×3 integration points.

A typical finite element mesh is shown in figure 3: symmetry has been used to reduce the number of degrees of freedom. A fine mesh is required to resolve the steep stress and displacement gradients near the edge of the contact area. A unit vertical displacement was enforced over the area of contact: in the case of the bonded punch, the tangential displacements in the contact area were also set to zero. For the axisymmetric case, numerical experiments showed that the results are not very sensitive to the far-field boundary conditions, provided that the boundary is sufficiently far from the contact area. A distance of $20a$ was found to give good results. In this case, we have enforced zero displacement perpendicular to the remote boundary, and no traction parallel to it. For the plane punch, the displacements decay slowly with distance from the punch, particularly when m is close to 1, so that the results are very sensitive to remote boundary conditions. The distance to the boundary of the finite element mesh was therefore extended to $40a$, and the tractions associated with a point load acting at the origin were enforced around the boundary. Expressions for the tractions may be deduced from the results for a point load on a power-law elastic solid given in Johnson (1985). The magnitude of the remote tractions consistent with a unit displacement of the punch cannot easily be calculated. We avoided this difficulty by choosing an arbitrary value $L = 1000$ for the magnitude of the point load, and scaled the numerical results so as to give a unit displacement under the punch. As m is increased, the results become less sensitive to the remote boundary conditions. For values of $m > 5$, we found no appreciable difference between results obtained with tractions specified around the boundary, and results with zero normal displacement perpendicular to the boundary. We found it more convenient to prescribe remote displacement boundary conditions in this case.

The functions $c(m, n)$ and $F_a(m)$ and $F_p(m)$ have been found using results from the finite element calculations. F_a and F_p correspond to the loads on the flat punch, and were evaluated by expressing the load as a volume integral using the principle of virtual work. The volume integral was evaluated by numerical quadrature. To calculate c, the integral in (1.13) was evaluated numerically, using a piecewise-quadratic integration formula consistent with the finite element interpolation functions. For the axisymmetric punch, the integral was truncated at the edge of the finite element mesh. This procedure does not give accurate results for the plane punch, since the displacements $U(\hat{r})$ decay too slowly with $\hat{r}$. In this case, the integral in (1.13) was divided into two contributions:

$$c^n = 1 - n\int_1^{\hat{R}} \frac{U_3(\hat{r})}{\hat{r}^{n+1}}\,\mathrm{d}\hat{r} - n\int_{\hat{R}}^{\infty} \frac{U_3(\hat{r})}{\hat{r}^{n+1}}\,\mathrm{d}\hat{r}, \tag{2.64}$$

where $\hat{R}$ is the position of the edge of the finite element mesh. The first integral in (2.64) was evaluated numerically, using the finite element results. The second integral was evaluated in closed form, using the solution for a point load on a nonlinear elastic half-space. The function $b(m, n)$ in equation (2.40) and the surface displacements in (2.37) were calculated using the same procedure.

In principle, the full displacement field in the solid may be calculated from the flat punch solution, using equation (2.36). However, a rather cumbersome interpolation scheme is required to calculate displacements at arbitrary points within the finite element mesh. We have found it more convenient to calculate the displacements using full-field finite element solutions, obtained using the commercial finite element code ABAQUS. Since the displacement fields are known to scale according to equations (1.10) and (1.11), it is only necessary to calculate one solution for a particular indenter geometry and value of m. In the full-field simulations, a finite strain elastic-creeping constitutive model was used, given by

$$\dot{\epsilon}_{ij} = \left(\frac{1+\nu}{E}\delta_{ik}\delta_{jl} - \frac{\nu}{E}\delta_{ij}\delta_{kl}\right)\overset{\nabla}{\sigma}_{kl} + \tfrac{3}{2}\dot{\epsilon}_0\left(\frac{\sigma_e}{\sigma_0}\right)^{m-1}\frac{S_{ij}}{\sigma_0}. \tag{2.65}$$

Here, E is Young's modulus, and ν is Poisson's ratio, while $\dot{\epsilon}_{ij}$ denotes the rate of deformation, and $\overset{\nabla}{\sigma}_{ij}$ is the Jaumann rate of Cauchy stress. We have used values of $E = 1000$, $\nu = 0.3$, $\dot{\epsilon}_0 = 0.1$ and $\sigma_0 = 1$ in our calculations: these values are such that elasticity has a negligible effect on the results. A mesh consisting of 701 four noded hybrid quadrilateral elements was used to interpolate the displacement field in the half-space. The diameter of the indenter was chosen to be 20–200 times the smallest element size.

3. Results and Discussion

(*a*) *Indentation load*

To interpret the results of a hardness test on a creeping solid, it is the variation of load L with penetration depth h and indentation rate $\dot{h}$ that is of greatest interest. The scaling procedure described in the preceding sections shows that the load can be expressed in terms of functions $F_a(m)$ and $F_p(m)$ as given in equation (1.6). The dimensionless contact pressures $F_a(m)$ and $F_p(m)$ have been calculated using the finite element method, and are shown in figure 4. Numerical values of F have been tabulated in tables 1–4.

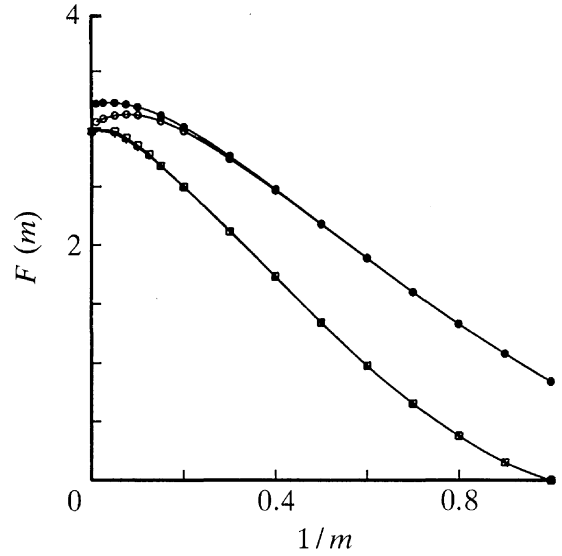

Figure 4. Variation of reduced contact pressure $F_a(m)$ and $F_p(m)$ with strain rate exponent m. ○, Axisymmetric frictionless; +, plane frictionless; ●, axisymmetric bonded; □, plane bonded.

Table 1. *Results for an axisymmetric frictionless indenter*

$1/m$	$c(m,1)$ cone	$c(m,2)$ sphere	$b(m,1)$ cone	$b(m,2)$ sphere	$F_a(m)$
1.00	0.636	0.707	0	0	0.849
0.90	0.692	0.747	0.009	0.009	1.085
0.80	0.745	0.788	0.020	0.022	1.332
0.70	0.802	0.831	0.032	0.037	1.602
0.60	0.859	0.875	0.047	0.058	1.886
0.50	0.916	0.920	0.065	0.084	2.176
0.40	0.974	0.966	0.087	0.118	2.465
0.30	1.033	1.013	0.115	0.164	2.734
0.20	1.097	1.065	0.151	0.227	2.973
0.10	1.174	1.128	0.203	0.323	3.110
0.01	1.263	1.201	0.262	0.442	3.051

Table 2. *Results for an axisymmetric bonded indenter*

$1/m$	$c(m,1)$ cone	$c(m,2)$ sphere	$b(m,1)$ cone	$b(m,2)$ sphere	$F_a(m)$
1.00	0.643	0.709	0	0	0.848
0.90	0.692	0.747	0.008	0.007	1.085
0.80	0.745	0.788	0.017	0.017	1.332
0.70	0.801	0.830	0.028	0.030	1.603
0.60	0.857	0.874	0.041	0.047	1.888
0.50	0.914	0.918	0.056	0.070	2.182
0.40	0.970	0.962	0.076	0.099	2.476
0.30	1.027	1.008	0.099	0.137	2.758
0.20	1.085	1.054	0.128	0.186	3.007
0.10	1.148	1.105	0.162	0.247	3.182
0.01	1.209	1.155	0.195	0.312	3.212

The accuracy of the finite element results may be estimated by comparing them to the exact solutions for $m = 1$ and $m = \infty$ given in §2*b*: the numerical results differ from the exact solution by less than 0.5%. Results are shown in figure 4 for both

Table 3. *Results for a plane frictionless indenter*

$1/m$	$c(m,1)$ wedge	$c(m,2)$ cylinder	$b(m,1)$ wedge	$b(m,2)$ cylinder	$F_p(m)$
1.0	0	0	0	0	0
0.9	0.156	0.323	0.003	0.002	0.151
0.8	0.308	0.465	0.012	0.009	0.375
0.7	0.452	0.578	0.028	0.023	0.655
0.6	0.588	0.678	0.051	0.045	0.9795
0.5	0.729	0.777	0.083	0.079	1.346
0.4	0.861	0.870	0.121	0.125	1.729
0.3	0.975	0.954	0.167	0.187	2.123
0.2	1.080	1.027	0.213	0.255	2.497
0.1	1.220	1.124	0.289	0.375	2.832
0	1.500	1.322	0.500	0.750	2.968

Table 4. *Results for a plane bonded indenter*

$1/m$	$c(m,1)$ wedge	$c(m,2)$ cylinder	$b(m,1)$ wedge	$b(m,2)$ cylinder	$F_p(m)$
1.0	0	0	0	0	0
0.9	0.156	0.323	0.002	0.001	0.151
0.8	0.308	0.465	0.011	0.007	0.375
0.7	0.451	0.577	0.025	0.019	0.655
0.6	0.586	0.677	0.045	0.037	0.979
0.5	0.720	0.772	0.073	0.065	1.342
0.4	0.854	0.866	0.108	0.107	1.732
0.3	0.959	0.943	0.147	0.158	2.114
0.2	1.069	1.019	0.191	0.219	2.497
0.1	1.198	1.107	0.251	0.309	2.849
0	1.333	1.208	0.333	0444	2.968

frictionless and perfectly bonded indenters. The load on a fully bonded indenter is marginally greater than for the frictionless case, but the influence of friction is small, particularly under a plane indenter. A surprising feature of the pressure under an axisymmetric punch is that $F_a(m)$ has a maximum value at $1/m \approx 0.15$. This behaviour was not observed for the plane indenter, where $F_p(m)$ appears to increase steadily as $1/m$ decreases.

(*b*) *Surface displacement field*

The variation of the radius of contact a with penetration depth h is also of interest. It has been shown that a is related to h by the constant c defined in equation (1.5). The variation of c with hardening exponent m has been calculated from our finite element results, and is plotted in figure 5. In addition, numerical values are given in tables 1–4. Results are shown for two values of the indenter parameter n defined in equation (1.4). The case $n = 1$ corresponds to a cone (in the axisymmetric case) or a wedge (for the plane punch), while $n = 2$ is representative of a spherical or cylindrical indenter. We have seen that c has two physical interpretations: it corresponds to the ratio of the true to nominal contact radius, and also determines the vertical displacement of material at the edge of the contact area, as given in equation (2.39). Figure 5 shows that $c > 1$ for $1/m < 0.3$, implying that material piles up at the edge of the area of contact. As $1/m$ increases beyond this point, material tends to be

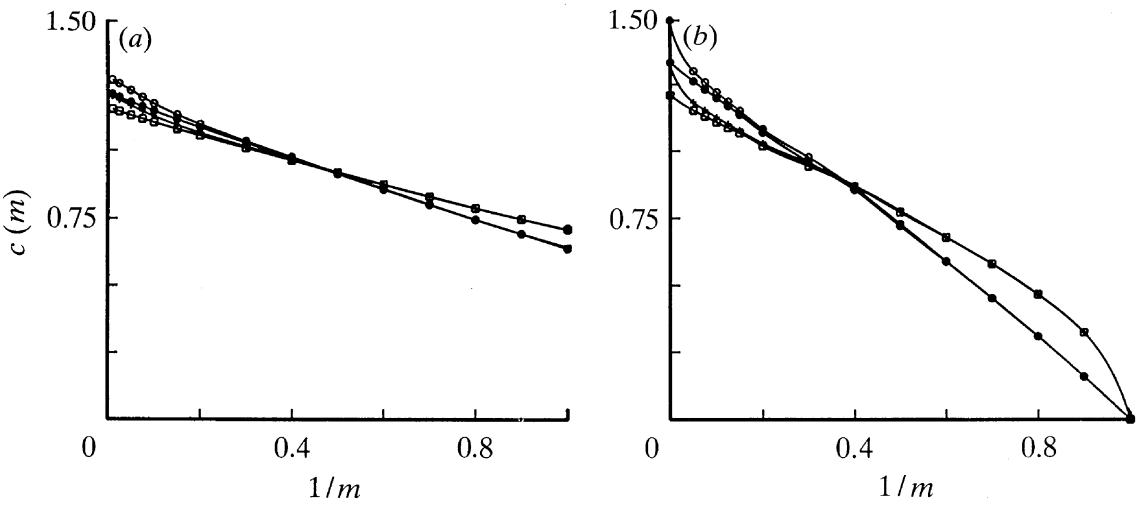

Figure 5. Variation of ratio of true to apparent contact area c with strain rate exponent m. (a) Axisymmetric punch: ○, frictionless cone ($n = 1$); +, frictionless sphere ($n = 2$); ●, bonded cone ($n = 1$); □, bonded sphere ($n = 2$). (b) Plane punch: ○, frictionless wedge ($n = 1$); +, frictionless cylinder ($n = 2$); ●, bonded wedge ($n = 1$); □, bonded cylinder ($n = 2$).

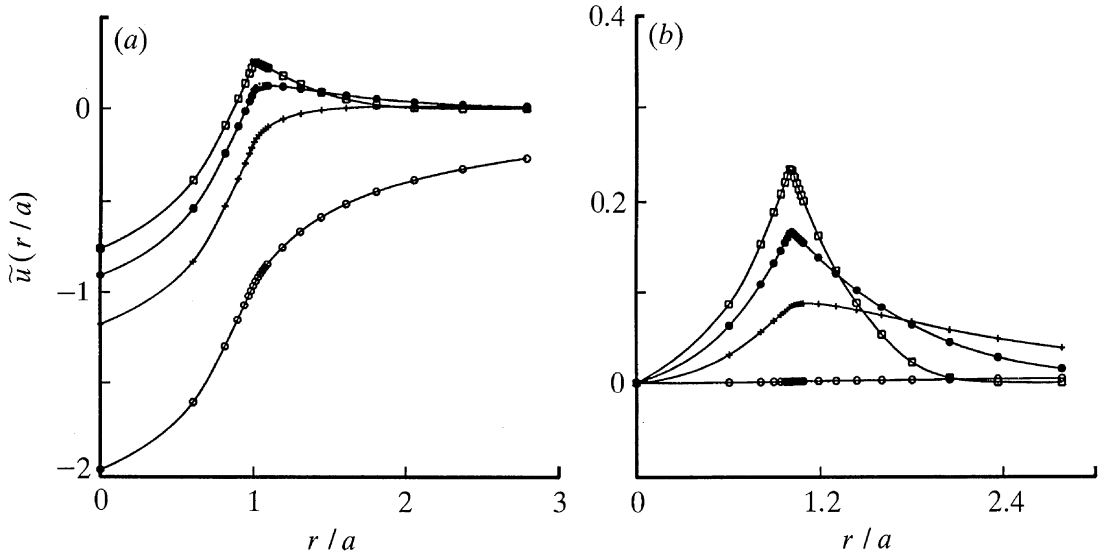

Figure 6. Displacement of the surface near a spherical indenter, assuming no slip in the area of contact. (a) Vertical displacement. (b) Radial displacement. ○, $m = 1$; +, $m = 2$; ●, $m = 5$; □, $m = 100$.

pushed into the surface of the half-space. This behaviour is illustrated in figure 6a, which shows the vertical displacement of the surface caused by indenting the solid with a sphere, for four values of m. Results are shown for the fully bonded case. The displacements have been presented in dimensionless form by plotting the transformed displacements $\tilde{u}_i(r/a)$. The displacement field for a particular ball diameter and indentation depth can be deduced using the scaling given in equation (1.10). Similar results were reported by Hill *et al.* (1989) in their analysis of indentation of a power-law elastic solid by a sphere. Indeed, for spherical indentation, our values of c as a function of the strain rate exponent m are very similar to those of Hill and co-workers, who found c as a function of the strain hardening exponent.

The radial displacement of material at the edge of the contact area also varies linearly with indentation depth. Its magnitude is determined by the constant b defined in equation (2.40), which depends only on m and n. The variation of b with

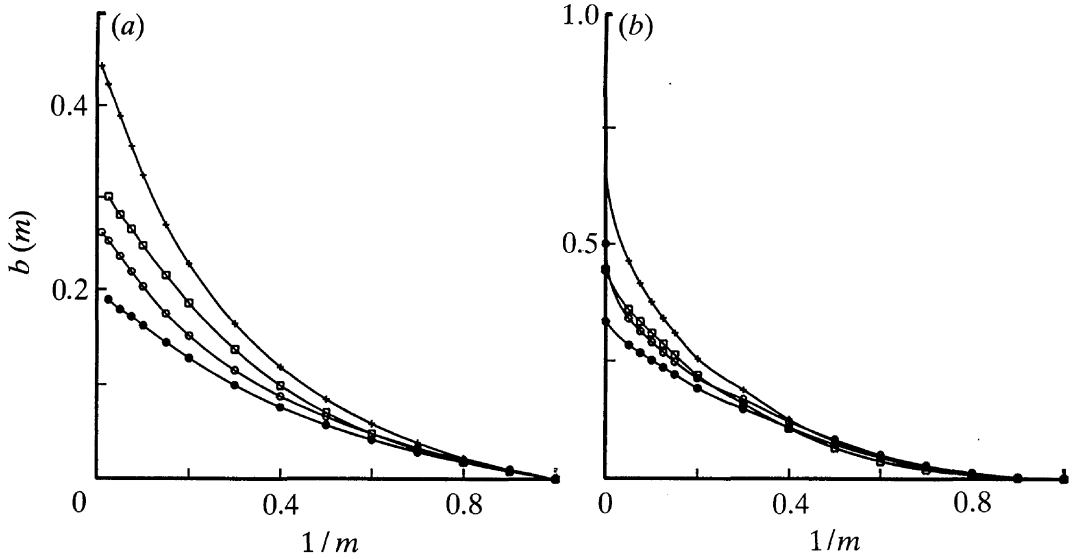

Figure 7. Variation of ratio of tangential displacement at edge of contact area to penetration depth $b(m)$ with strain rate exponent m. (*a*) Axisymmetric punch: ○, frictionless cone ($n = 1$); +, frictionless sphere ($n = 2$); ●, bonded cone ($n = 1$); □, bonded sphere ($n = 2$). (*b*) Plane punch: ○, frictionless wedge ($n = 1$); +, frictionless cylinder ($n = 2$); ●, bonded wedge ($n = 1$); □, bonded cylinder ($n = 2$).

$1/m$ is plotted in figure 7, for values of n representative of spherical and conical indenters, and also for wedge and cylindrical plane punches. The results are strongly dependent on friction, which suggests a possible way of estimating the frictional conditions in experiments. For reference, the variation of tangential displacement at the surface is shown in figure 6*b*, for the case of indentation by a fully bonded sphere. The displacements inside the area of contact clearly have the parabolic distribution predicted by equation (2.41).

(*c*) *Contact stress distribution*

The finite element computations also enable the stress and strain fields under the indenter to be examined in detail. The distribution of contact pressure is of particular interest, and is shown for an axisymmetric indenter in figure 8. The figure shows the variation of the transformed contact pressure $P(r/a)/F(m)$: the actual contact pressure for a particular indenter and material may be deduced using the scaling in equation (2.34). For comparison, the exact solution for $m = 1$ has also been plotted on figure 8: our numerical calculations agree well with the exact result. For $m < \infty$, the contact pressure is singular at the edge of the punch. The asymptotic variation of $P(r/a)$ as $r \to \pm a$ can be deduced from the results of studies of the stress field near the tip of a crack in a power law hardening solid. It has been shown that the stress and strain rate fields in the creeping solid are equivalent to those in a power law elastic half-space indented by a rigid flat punch. The problem of an external crack in a power law hardening solid has the same boundary conditions. For the frictionless indentation problem, the boundary conditions correspond to those for an external circular crack (axisymmetric case) or an external slit crack (for the plane case) in a power-law elastic body. For both geometries, the stress field near the crack tip has the form (Hutchinson 1968; Rice & Rosengren 1968)

$$P(r/a) = \left(\frac{J}{1-|r/a|}\right)^{1/(m+1)} f(m). \tag{3.1}$$

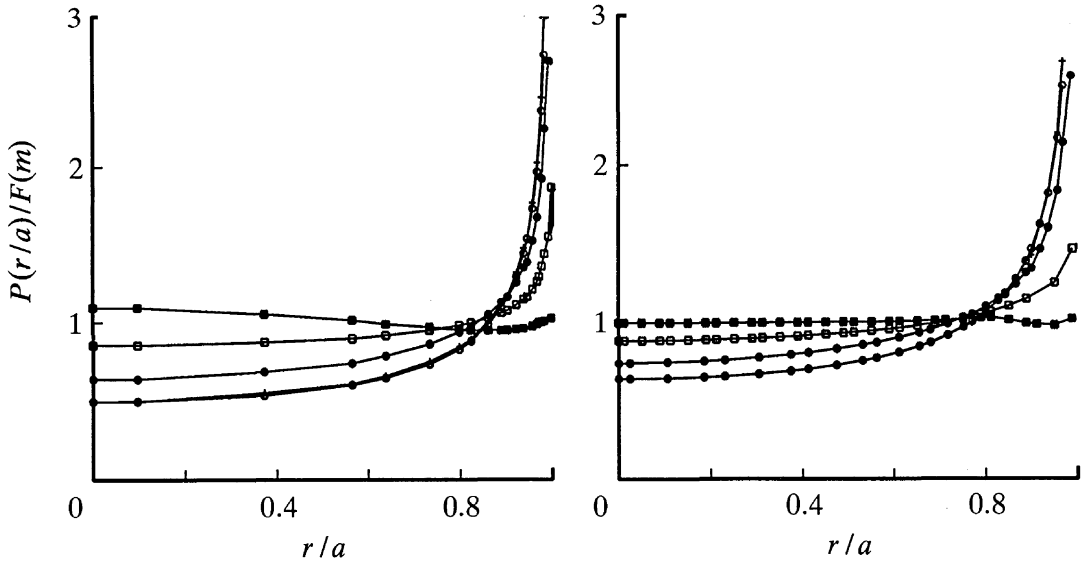

Figure 8. Distribution of contact pressure under an indenter. (*a*) Frictionless axisymmetric indenter. (*b*) Frictionless plane indenter. ○, $m = 1$ (exact); +, $m = 1$ (numerical); ●, $m = 2$; □, $m = 5$; ■, $m = 100$.

Here, J is the energy released per unit length of crack front due to an infinitesimal crack advance, and $f(m)$ is a bounded function. It is straightforward to relate J to the load applied to the punch, with the result

$$J = \frac{2m-1}{2+2m} F_a(m), \quad \text{axisymmetric punch,} \tag{3.2}$$

$$J = \frac{m-1}{1+m} F_p(m), \quad \text{plane punch.} \tag{3.3}$$

Equation (3.1) indicates that as m increases, the strength of the singularity in contact pressure at the edge of the punch diminishes. Our numerical results illustrate this trend. As $m \to \infty$ the contact pressure becomes bounded at $r = \pm a$. In principle, the stress distribution should approach the results for indentation of a rigid perfectly plastic solid as $m \to \infty$. For the plane punch, the pressure tends to a uniform distribution, as predicted by the slip line field solutions discussed in §2. The contact pressure does not appear to tend to a uniform value under an axisymmetric indenter. This is consistent with the results obtained by Hill *et al.* (1990), who calculated the contact pressure distribution under a sphere indenting a power-law elastic half-space. In their solution, the contact pressure is zero at the edge of the punch, even as the rigid plastic-limit is approached. This does not appear to be the case in our results: the contact pressure $P(r/a)/F(m)$ exceeds unity for $r > 0.95a$ for both $m = 100$ and $m = 1000$. However, it is likely that the stress distribution converges to the rigid plastic limit very slowly as m increases.

For the perfectly bonded punch, the boundary conditions correspond to those for a crack in the interface between a power-law hardening solid and rigid substrate. The asymptotic fields for this configuration have been examined by Sharma & Aravas (1992). The field near the crack tip is of the form (3.1), where J is given by (3.2) and (3.3). This singular field exists for a single mode mix, the value of which depends on m. However, the field is close to mode I in nature for all values of m. Sharma & Aravas (1993) and Shih (1991) show that the region of dominance of the asymptotic

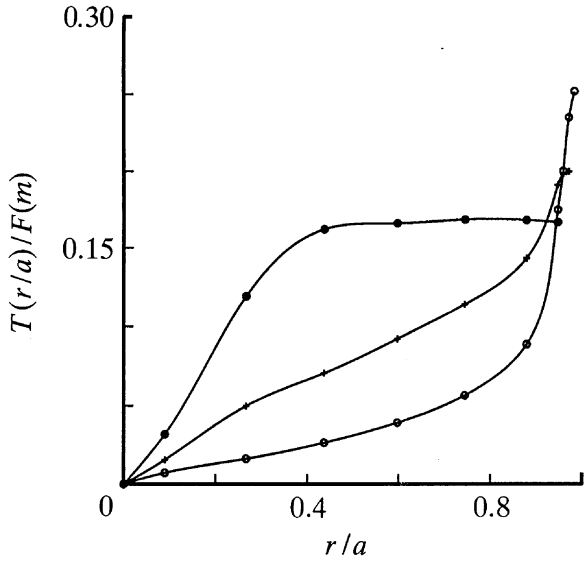

Figure 9. Distribution of surface traction under a bonded axisymmetric indenter. ○, $m = 2$; +, $m = 5$; ●, $m = 100$.

solution is much smaller than all length scales of physical relevance. In practice, the indenter is unlikely to remain perfectly bonded to the half-space close to the edge of the punch, so that the crack tip field is not a good approximation. However, the behaviour is qualitatively similar to the results for a frictionless indenter, and the expressions for the energy release rate J also apply to the sticking punch.

For the bonded punch, it is instructive to examine the variation of tangential traction inside the area of contact. The traction under an axisymmetric indenter is shown in figure 9. We have plotted the reduced tangential tractions $T(r/a)/F(m)$: the actual traction for a particular material and indentation rate can be calculated using the same scaling as for the contact pressure, given in (2.34). The traction is zero for $m = 1$, but its magnitude increases with m. In our calculations, we have assumed that the punch is perfectly bonded to the half-space. If the coefficient of Coulomb friction is finite, there is always a small region near the edge of the contact where slip occurs, provided $m \neq 1$. However, the region of slip is small: if the friction coefficient $\mu > 0.17$, the size of the region of slip at the edge of the contact is less than $0.1a$, for both axisymmetric and plane indenters. For the slip region to extend over a region $0.9a$, the friction coefficient must be less than 0.05. Consequently, it is probable that the results for fully bonded indenters are more representative of experiments than those for the frictionless case.

As an indication of the distributions of strain the creeping solid, we have plotted contours of accumulated von-Mises equivalent strain under a frictionless spherical indenter in figure 10. We have plotted the normalized strains $\tilde{\epsilon}_a = (D/a)\int (\frac{2}{3}\dot{\epsilon}_{ij}\,\dot{\epsilon}_{ij})^{\frac{1}{2}}\,\mathrm{d}t$, so that the results are independent of the ball diameter and contact radius. The strain levels for any combination of sphere diameter and contact radius can be calculated using the scaling in equation (1.11). For m close to 1, the maximum strain is located on the axis of symmetry, but as m increases, the maximum strain shifts towards the edge of the contact. The contours differ significantly from the corresponding results for indentation of a power-law elastic solid given by Hill *et al.* (1990). They differ partly because we have plotted the accumulated Mises strain, rather than the value of $\tilde{\epsilon}_e = (\frac{2}{3}\tilde{\epsilon}_{ij}\,\tilde{\epsilon}_{ij})^{\frac{1}{2}}$, computed from the current reduced strain components. Since the loading is non-proportional, the two measures of strain are not equivalent. Contours of reduced von-Mises strain rate $E_e = (\frac{2}{3}E_{ij}E_{ij})^{\frac{1}{2}}$ have been

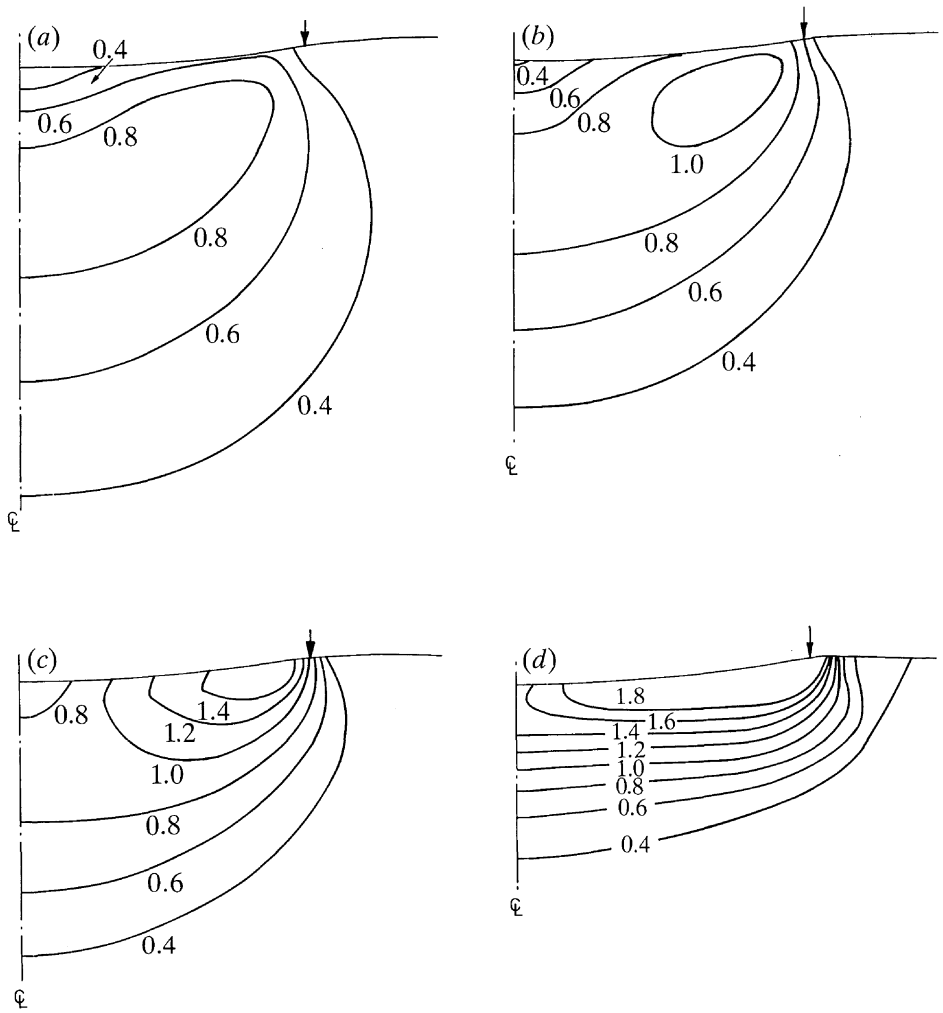

Figure 10. Contours of normalized von-Mises accumulated strain under a spherical frictionless indenter. The arrow marks the edge of the area of contact. (*a*) $m = 1$, (*b*) $m = 2$, (*c*) $m = 5$, (*d*) $m = \infty$.

plotted on figure 11 for comparison. The strain rate levels for any arbitrary indentation rate and contact radius can be deduced from the reduced strains using equation (1.9).

(*d*) *Predictions for a Vickers pyramid*

Although we have so far confined attention to axisymmetric and plane indenters, it is evident that a similar transformation procedure may be used to analyse other indenter geometries, provided that the shape of the contact remains self-similar with indentation depth. In particular, expressions of the form (1.5)–(1.11) can be found for a Vickers pyramid. For example, the load on a Vickers indenter scales as

$$L/4a^2\sigma_0 = (\dot{h}/a\dot{\epsilon}_0)^{1/m} F_v(m), \tag{3.4}$$

where a is half the length of one side of the contact. The function F_v corresponds to the load applied to a flat square punch of size 2×2, which is pressed to a unit depth into a nonlinear elastic solid. This problem has not been solved for arbitrary m, but we may obtain an estimate for F_v by assuming that the load on the flat punch scales with the square root of the area of contact, and is independent of the shape of the contact. This gives $F_v(m) = \frac{1}{2}F_a(m)\sqrt{\pi}$. The accuracy of this approximation may be estimated using a solution to the square punch problem for $m = 1$, given by King

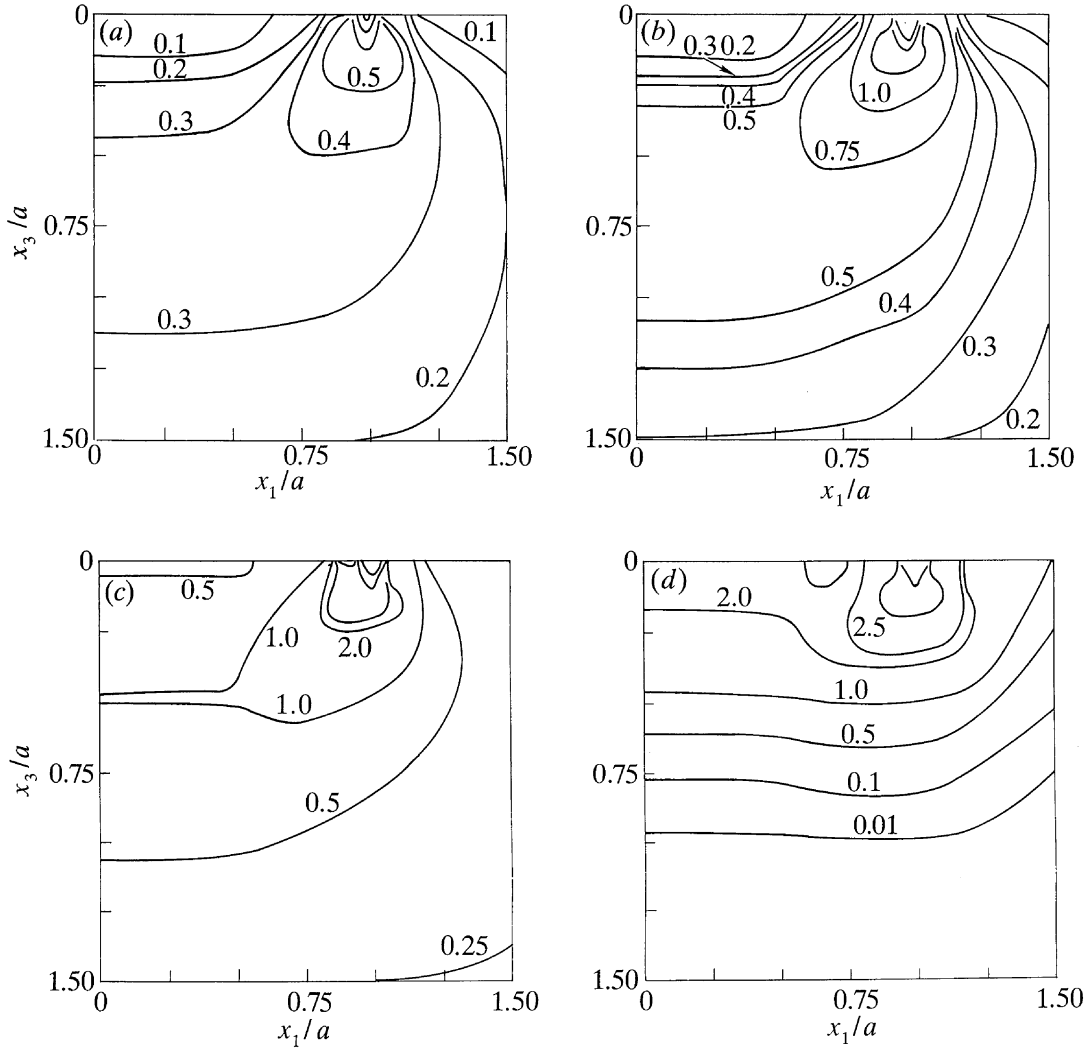

Figure 11. Contours of reduced von-Mises equivalent strain rate under an indenter. (*a*) $m = 1$, (*b*) $m = 2$, (*c*) $m = 5$, (*d*) $m = 100$.

(1987). The accurate solution leads to $F_v(1) = 0.7605$, while our estimate gives $F_v(1) = 0.7522$: the accuracy of the approximation should improve as m increases. In addition, the value of c for a pyramid is likely to be close to our results for a cone.

(*e*) *The concept of equivalent stress and strain under an indenter*

The results of hardness tests on creeping materials are usually interpreted using Mulhearn & Tabor's (1960) concepts of 'effective stress' and 'effective strain rate' under the indenter, outlined in the introduction. The effective stress is taken to be proportional to the contact pressure, while the effective strain rate is determined by the shape of the indenter and indentation rate. The effective stress is assumed to be related to the effective strain rate by the uniaxial stress–strain response (1.1). This procedure is fully justified in the light of our calculations. For example, for a conical indenter with included angle 2β, equations (1.5) and (1.6) may be combined to give

$$L/\pi a^2\sigma_0 = F_a(m)\,(\dot{h}/\dot{\epsilon}_0\, ch \tan\beta)^{1/m}. \tag{3.5}$$

This expression has the form of equation (1.2), with $\alpha = F(m)$, $\gamma = 1/c(m)$ and $\dot{\epsilon}^{\text{eff}} = \dot{h}/h\tan\beta$. Alternatively, for a spherical indenter diameter D we may put

$$L/\pi a^2\sigma_0 = F_a(m)\,(2\dot{a}/\dot{\epsilon}_0\, c^2 D)^{1/m}. \tag{3.6}$$

This is consistent with the formula in (1.2), and justifies Mulhearn & Tabor's (1960) use of $\dot{\epsilon}^{\text{eff}} = \dot{a}/D$. However, it should be recognized that the form of equations (3.5) and (3.6) is a consequence of the properties of the stress and deformation fields in a power-law creeping material. The concepts of effective stress and effective strain under an indenter cannot necessarily be extended to materials which do not have a uniaxial stress–strain response of the form (1.1).

(*f*) *Comparison with experiment*

The predictions of our analysis may be compared with the results of experiments. The simplest hardness test on a creeping solid involves applying a constant load L to the indenter, and measuring the variation of contact pressure $L/\pi a^2$ as a function of time (Mulhearn & Tabor 1960; Atkins *et al.* 1966). Our calculations predict that for such a test, the contact pressure varies with time t as

$$L/\pi a^2 = \begin{cases} C_{\mathrm{c}}\, t^{-1/m}, & \text{conical indenter,} \\ C_{\mathrm{s}}\, t^{-2/(2m+1)} & \text{spherical indenter,} \end{cases} \tag{3.7}$$

with C_{c} and C_{s} being constants which depend on material properties and the geometry of the indenter. For a material with high m, the variation of C_{c} and C_{s} with indenter geometry is small, and in both cases pressure is proportional to $t^{-1/m}$. This behaviour is in good agreement with experimental measurements by Mulhearn & Tabor (1960) and Atkins *et al.* (1966), who have shown that a plot of log (pressure) against log (time) in a straight line, with slope $-1/m$. Further support for our analysis may be found in Mayo & Nix (1988), who have used a nanoindenter to measure the variation of pressure with $\dot{h}/h$ for a number of different materials. Their results indicate a power-law dependence which is in excellent agreement with the predictions of (1.5) and (1.6).

(*g*) *Limitations of the theory*

The agreement between theory and experiment suggests that our model is representative of practical hardness tests. Nevertheless, it is instructive to investigate the limitations of the theory. Three assumptions in particular may lead to difficulties. First, we have neglected the effects of elasticity in our calculations, and secondly, the power-law creep model used here may over-simplify the behaviour of the material. Finally, our calculations have assumed that all the displacements and strains remain small during the indentation. The effects of these approximations are considered in turn below.

(i) *The influence of elasticity*

A simple analysis may be used to estimate the conditions where elasticity is likely to have a significant effect on our results. For simplicity, assume that the deforming material is an incompressible elastic-creeping solid, with a constitutive law given by

$$\dot{\epsilon}_{ij} = \frac{3}{2E}\dot{S}_{ij} + \tfrac{3}{2}\dot{\epsilon}_0 \left(\frac{\sigma_e}{\sigma_0}\right)^{m-1} \frac{S_{ij}}{\sigma_0}, \tag{3.8}$$

where E is Young's modulus. Suppose that an axisymmetric indenter with a profile of the form (1.4) is pushed into the surface of the half-space at a constant rate $\dot{h}$. The resulting displacement field in the solid may be thought of as the sum of an elastic component u_i^{e} and a plastic part u_i^{p}. If $u^{\mathrm{e}} \ll u^{\mathrm{p}}$, then the effects of elasticity may be

neglected. The relative magnitudes of the two components may be estimated as follows. In the absence of elasticity, the load on the punch is given by equations (1.6) and (1.7). If the same load were applied to a flat punch of radius a indenting an incompressible linear elastic half-space, the maximum displacement of the surface would be

$$\frac{h^{\mathrm{e}}}{a} = \frac{L}{\pi a^2 E F_a(1)} = \frac{\sigma_0}{E}\left(\frac{\dot{h}}{a\dot{\epsilon}_0}\right)^{1/m} \frac{F_a(m)}{F_a(1)}. \tag{3.9}$$

As long as the actual indentation depth h exceeds the 'elastic' indentation depth h^{e} by a sufficient margin, the elastic component of the displacement field may be neglected. The ratio $\Lambda = F_a(m)\,h/F_a(1)\,h^{\mathrm{e}}$ is a convenient measure of the influence of elasticity. From (3.9), Λ is given by

$$\Lambda = \frac{E\dot{\epsilon}_0^{1/m}}{\sigma_0}\frac{h}{a}\left(\frac{a}{\dot{h}}\right)^{1/m}. \tag{3.10}$$

The effects of elasticity may be neglected if $\Lambda \gg 1$.

The effects of elasticity may be examined in more detail using solutions to the limiting cases of a linear viscoelastic solid, and an elastic–perfectly-plastic material. Consider first indentation of an incompressible linear viscoelastic solid. The constitutive model for such a material is given by (3.8), with $m = 1$. Suppose that an indenter is pressed into the surface of the solid at a constant rate $\dot{h}$. The method outlined by Lee & Radok (1960) may be used to solve this problem. The analysis shows that the area of contact is related to the indentation depth through equation (1.5) throughout the period of loading. The values of c given in equation (2.46) for a linear viscous solid apply equally well for the viscoelastic case. However, the load L on the indenter varies with time t, and may be expressed as

$$L/\pi a^2\sigma_0 = (\dot{h}/a\dot{\epsilon}_0)\,F_a(1)\,G(t/T, n). \tag{3.11}$$

Here, T is a material time constant, given by $T = \sigma_0/(E\dot{\epsilon}_0)$, and $G(\tau, n)$ is a dimensionless function which depends on the geometry of the indenter through n. For conical and spherical indenters, G may be shown to be

$$G(\tau, 1) = 1 + (1/\tau)\,(\exp(-\tau) - 1), \qquad \text{cone} \tag{3.12}$$

$$G(\tau, 2) = 1 + \tfrac{1}{2}\mathrm{i}\sqrt{(\pi/\tau)}\,\mathrm{erf}(\mathrm{i}\sqrt{\tau})\exp(-\tau), \qquad \text{sphere}, \tag{3.13}$$

where $\mathrm{i} = \sqrt{(-1)}$ and $\mathrm{erf}(x)$ denotes the error function. It is evident that $G(\tau, n) \to 1$ as $\tau \to \infty$, in which case (3.11) approaches the limit (1.6) for a pure creeping solid. Elasticity gives rise to a transient solution with a time constant T: evaluating G shows that the contact pressure differs from its steady state value by less than 5% for $t/T > 15$ for a cone, and $t/T > 20$ for a sphere.

To interpret these results in terms of the parameter Λ defined earlier, we note that for $m = 1$, Λ is given by

$$\Lambda(m = 1) = \frac{E\dot{\epsilon}_0}{\sigma_0}\frac{h}{\dot{h}} = \frac{1}{T}\frac{h}{\dot{h}}. \tag{3.14}$$

Since $h/\dot{h} = t$ for a constant rate of penetration, the condition $\Lambda \gg 1$ is equivalent to $t/T \gg 1$. It appears that for $m = 1$, elasticity may be neglected for both conical and spherical indenters if $\Lambda > \Lambda_{\mathrm{crit}}$ where $\Lambda_{\mathrm{crit}} \approx 20$.

The influence of elasticity in the rate independent limit $m = \infty$ is discussed at length by Johnson (1985). It appears that equations (1.5) and (1.6) predict correctly

the area of contact and pressure under the indenter provided that the plastic strains exceed the elastic strains by a sufficient margin. Johnson (1985) suggests that the relative magnitudes of the strains are governed by a dimensionless parameter λ which depends on the geometry of the indenter. For the indentation of an incompressible elastic–perfectly-plastic solid, λ is given by

$$\lambda = \begin{cases} 4E/3\sigma_0 \tan\beta, & \text{conical indenter,} \\ 8Ea/3D\sigma_0, & \text{spherical indenter,} \end{cases} \tag{3.15}$$

where σ_0 is the tensile yield stress of the solid. Johnson argues that the effects of elasticity may be neglected if $\lambda > 30$ for a cone, and $\lambda > 40$ for a sphere. These results may be interpreted in terms of the parameter Λ defined in (3.10). For $m = \infty$, the parameter reduces to

$$\Lambda(m = \infty) = hE/a\sigma_0. \tag{3.16}$$

Using equation (1.5) together with the results shown in figure 5, we find that $h/a \approx 1/1.2\tan\beta$ for a conical indenter, and $h/a \approx a/1.4D$ for a spherical indenter. Substituting these values in (3.16) shows that, apart from a numerical factor, Johnson's geometrical parameter is equivalent to Λ in the rate independent limit. Furthermore, using Johnson's estimates for the critical value of λ, we find that elasticity may be neglected in the rate independent limit if $\Lambda > \Lambda_{\text{crit}} \approx 20$ for a cone, and $\Lambda > \Lambda_{\text{crit}} \approx 30$ for a sphere.

We have investigated the influence of elasticity in the range $1 < m < \infty$ using full-field finite element calculations. The results show that for $m = 2$, the elastic-creeping solution is within the 5% of the rigid-creep solution if $\Lambda > \Lambda_{\text{crit}} = 25$ for a spherical indenter, and $\Lambda > \Lambda_{\text{crit}} = 18$ for a cone. Thus, if $\Lambda > 30$ elasticity may be neglected for both indenter geometries throughout the range $1 < m < \infty$.

(ii) *The power-law creep assumption*

The applicability of a power-law creep model under the conditions of a hardness test is open to question. Strictly, equation (1.3) is designed to predict the strain rate in a solid subjected to a constant stress. It has been suggested that since material elements under the indenter are subjected to a complex history of stress, a transient creep law should be used to model the solid (Atkins *et al.* 1966). However, our results indicate that most of the material under the indenter is in fact subjected to a constant level of equivalent stress. The stress history for elements of material under the contact can be estimated using the contours of von-Mises strain rate plotted in figure 11. The equivalent stress is related to E_{e} by $\Sigma_{\text{e}} = E_{\text{e}}^{1/m}$. It is evident that for practical values of $m \geqslant 5$, there is a large area under the contact where the equivalent stress does not vary significantly. Thus, even though the size of the contact increases during loading, material elements under the indenter are subjected to an approximately constant level of equivalent stress.

(iii) *The influence of finite deformations*

We have examined the accuracy of the small strain theory by comparing the predictions with full field finite element calculations which take into account the effects of finite deformations. In the full-field simulations, we have investigated the deformation caused by a frictionless, spherical indenter which is pushed at constant speed into a power-law creeping solid. The numerical calculations are described in more detail in §2*c*. To compare the results with the small strain theory, we have

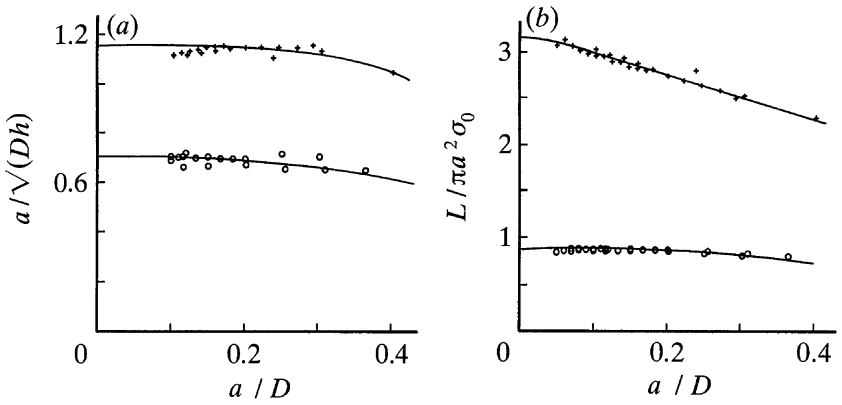

Figure 12. Results of full field finite element simulations of indentation by a sphere, including the effects of finite deformation. (*a*) Dimensionless contact radius $a/\sqrt{(Dh)}$ against a/D. (*b*) Contact pressure $L/\pi a^2$ against a/D. ○, $m = \infty$; +, $m = 1$.

plotted the predicted variation of $c = a/\sqrt{(Dh)}$ and $F_a = L/\pi a^2\sigma_0$ with contact radius a/D in figure 12. Results are shown for $m = 1$ and $m = \infty$. The numerical values of c and F fluctuate slightly as successive nodes in the finite element mesh come into contact with the indenter. In addition, data have not been plotted for values of $a/D < 0.1$, since significant errors are present in our results in this range due to the size of the finite element mesh.

According to the small strain theory, both c and F are independent of contact radius. The full field simulations show that for $a/D < 0.2$, the values of c and F are constant, and are equal to the predictions of the small-strain theory. The effects of finite strains become important for $a/D > 0.2$, and both c and F tend to decrease with increasing a/D beyond this point. We conclude that the predictions of the theory based on small strains are satisfactory for contact sizes up to $a/D = 0.2$.

A.F.B. is pleased to acknowledge support from I.B.M. Thomas J. Watson Research Center. A.N. is grateful for support provided by the Brown University Materials Research Group on the Micromechanics of Failure Resistant Materials, funded by the National Science Foundation. N.O. thanks the Association of Commonwealth Universities for support through a Commonwealth scholarship.

References

Atkins, A. G., Silvério, A. & Tabor, D. 1966 Indentation hardness and creep of solids. *J. Inst. Metals* **94**, 369.

Fabrikant, V. I. 1990 Complete solutions to some mixed boundary value problems in elasticity. *Adv. appl. Mech.* **27**, 153.

Hill, R. 1949 Plastic yielding of notched bars under torsion. *Q. J. Mech. appl. Math.* **2**, 40.

Hill, R. 1992 Similarity analysis of creep indentation tests. *Proc. R. Soc. Lond.* A **436**, 617–630.

Hill, R., Storåkers, B. & Zdunek, A. B. 1989 A theoretical study of the Brinell hardness test. *Proc. R. Soc. Lond.* A **423**, 301.

Hutchinson, J. W. 1968 Singular behaviour at the end of a tensile crack in a hardening material. *J. Mech. Phys. Solids* **16**, 13–31.

Johnson, K. L. 1970 The correlation of indentation experiments. *J. Mech. Phys. Solids* **18**, 115.

Johnson, K. L. 1985 *Contact mechanics*. Cambridge University Press.

King, R. B. 1987 Elastic analysis of some punch problems for a layered medium. *Int. J. Solids Struct.* **23**, 1657.

Lee, E. H. & Radok, J. R. M. 1960 The contact problem for viscoelastic bodies. *J. appl. Mech.* **27**, 438.

Marsh, D. M. 1964 Plastic flow in glass. *Proc. R. Soc. Lond.* A **279**, 420.

Matthews, J. R. 1980 Indentation hardness and hot pressing. *Acta metall.* **28**, 311.

Mayo, M. J. & Nix, W. D. 1988 A micro-indentation study of superplasticity in Pb, Sn, and Sn-38 wt % Pb. *Acta metall.* **36**, 2183.

Mulhearn, T. O. & Tabor, D. 1960 Creep and hardness of metals: a physical study. *J. Inst. Metals* **89**, 7.

Malkus, D. S. & Hughes, T. J. R. 1987 Mixed finite element methods – reduced and selective integration techniques: a unification of concepts. *Comput. Meth. appl. mech. Engng* **15**, 63–81.

Nix, W. D. 1989 Mechanical properties of thin films. *Metall. Trans.* A **20**, 2217.

Prandtl, L. 1920 *Göttinger Nachr. Math. Phys. Kl.* **74**, 37.

Rice, J. R. & Rosengren, G. F. 1968 Plane strain deformation near a crack tip in a power law hardening material. *J. Mech. Phys. Solids* **16**, 1–12.

Sargent, P. M. & Ashby, M. F. 1991 Indentation creep. In *Proc. Int. Colloq. Mechanics of creep of brittle materials 2* (ed. A. C. F. Cocks & A. R. S. Ponter), pp. 326–344. Elsevier Applied Science.

Sharma, S. M. & Aravas, N. 1993 On the development of variable-separable asymptotic elastoplastic solutions for interfacial cracks. *Int. J. Solids Structures.* (Submitted.)

Shih, C. F. 1991 Cracks on bimaterial interfaces: elasticity and plasticity aspects. *Mat. Sci. Engng* A **143**, 77–90.

Shih, C. F. & Needleman, A. 1984 Fully plastic crack problems, part I. *J. appl. Mech.* **100**, 48.

Sneddon, I. N. 1951 *Fourier transforms.* New York: McGraw-Hill.

Tabor, D. 1951 *Hardness of metals.* Oxford: Clarendon Press.

Wilkinson, D. S. & Ashby, M. F. 1975 Pressure sintering by power law creep. *Acta metall.* **23**, 1277.

Received 11 May 1992; accepted 29 October 1992